Hindawi
International Journal of Intelligent Systems
Volume 2023, Article ID 9381915, 14 pages
https://doi.org/10.1155/2023/9381915

Research Article

Artificial Neural Network-Based Experimental Investigations for Sliding Mode Control of an Induction Motor in Power Steering Applications

E. Parimalasundar,[1] R. Senthilkumar,[2] B. Hemanth Kumar,[1] K. Janardhan,[1] Arvind R. Singh,[3] Mohit Bajaj,[4,5,6] and Viktoriia Bereznychenko[7]

[1]*Department of Electrical and Electronics Engineering, Mohan Babu University (Erstwhile Sree Vidyanikethan Engineering College), Tirupati, India*
[2]*Department of EEE, SRM Institute of Science and Technology, Chennai, India*
[3]*Department of Electrical and Electronics Engineering, Koneru Lakshmaiah Education Foundation, Guntur, India*
[4]*Department of Electrical Engineering, Graphic Era (Deemed to be University), Dehradun 248002, India*
[5]*Graphic Era Hill University, Dehradun 248002, India*
[6]*Applied Science Research Center, Applied Science Private University, Amman 11937, Jordan*
[7]*Department of Theoretical Electrical Engineering and Diagnostics of Electrical Equipment, Institute of Electrodynamics, National Academy of Science of Ukraine, Peremogy, 56, Kyiv-57 03680, Ukraine*

Correspondence should be addressed to Viktoriia Bereznychenko; vika.vepsrf@gmail.com

Received 14 March 2023; Revised 17 May 2023; Accepted 10 August 2023; Published 11 October 2023

Academic Editor: Alexander Hošovský

Sliding mode control (SMC) of induction motor is a new concept in the current scenario, as it seeks to improve torque control accuracy and power steering efficiency through the use of pulse width modulation schemes. Furthermore, artificial neural network-based sliding mode control is applied to a squirrel cage induction motor, which is used in the steering control of automobiles. The artificial neural network (ANN)-based SMC is more popular due to its robustness and good stability in external parameter variation. Additionally, an SMC and an ANN-based SMC are employed to compute the torque and flux, improving performance for power steering applications. The performance of the designed model is validated through MATLAB/Simulink and experimental models with different controllers under various operating conditions. The controller has been embedded into a TMS320F28335 controller, and performances have been evaluated. The performance analyses of induction motor using different controllers are performed. The transient performances of induction motor such as delay time, rise time, settling time, and steady-state error are investigated. The proposed work is analysed by using a mathematical model and implemented in a test-bench model for validation.

1. Introduction

Induction motors (IMs) are widely used in various industrial and consumer applications due to their simple structure, robustness, and low cost. One of the significant applications of induction motors is power steering in automobiles, where they are used to provide the necessary torque to turn the wheels. The power steering system in modern cars is typically an electro-hydraulic system, where an electric motor drives a hydraulic pump to assist the driver in turning the wheels. In this application, the IM needs to be controlled precisely to ensure efficient and reliable operation. Sliding mode control (SMC) is a popular technique for controlling induction motors in various applications, including power steering. The idea behind sliding mode control is to design a controller that forces the system to slide along a specific surface, called the sliding surface, towards a desired state. Once the system reaches the sliding surface, it remains on it

and moves towards the desired state in a robust manner, regardless of disturbances or uncertainties.

High-order sliding modes (HOSM) are a class of control systems that are designed to provide robustness against uncertainties and disturbances in the system. This technique can be used to control a wide range of nonlinear systems, including mechanical systems, electrical systems, and chemical processes. HOSM controllers use a higher-order sliding surface compared to traditional sliding mode controllers, which can improve the performance and robustness of the system. In HOSM, the sliding surface is designed such that it passes through higher-order derivatives of the system state. There are two types of HOSM controllers: finite time and infinite time. Finite-time HOSM controllers aim to reach the sliding surface in a finite amount of time, while infinite-time HOSM controllers aim to stay on the sliding surface indefinitely. The high-order sliding mode manifold is well-defined as a solution to a high-order polynomial equation that depends on the system's state and its derivatives. The high-order sliding mode control technique can be used to control a wide range of nonlinear systems, including mechanical systems, electrical systems, and chemical processes. They are also able to achieve fast convergence to the sliding surface, leading to improved control performance. However, HOSM controllers can have some drawbacks [1, 2]. They require more complex control laws than traditional sliding mode controllers, which can make them more difficult to implement. Additionally, HOSM controllers can suffer from chattering, which is a high-frequency oscillation that can occur when the system approaches the sliding surface. This can be mitigated through the use of smoothing techniques, but this can add additional complexity to the controller design [3, 4].

Due to its simplicity, obvious performance, and performance, the proportional-integral (PI) regulator constitutes one of the most commonly employed methods of regulation in electrical machines [5]. An efficient nonlinear control may nevertheless enhance activity in an environment of issues and ambiguity since the IM operates within a nonlinear system [6, 7]. Several researchers have used a variety of cutting-edge control strategies to manage the power electronics and drive sector in this respect [8]. In particular, the sliding mode control [9–11], the predictive control approach [12–14], the adaptive control technique [15], and the backstepping algorithm [16–18] are involved in advanced electrical machine applications. With its unique dynamic characteristics for IM, such as robust reliability, rapid response, and straightforward software and hardware deployment, the SMC methodology has emerged as an intriguing nonlinear control method [19–21].

The sliding mode observer-based finite time control scheme is a method for controlling the frequency regulation and economic dispatch in power grids. It uses a sliding mode observer to estimate the states of the system, such as the generator speeds and power outputs, and then applies a finite time control scheme to adjust the control signals in order to regulate the frequency and optimize the economic dispatch [22, 23]. This method is effective in handling uncertainties and disturbances in the power grid, as the sliding mode observer is able to adapt to changing conditions and provide accurate state estimates. The finite time control scheme ensures that the system converges to the desired state in a finite time, which improves the stability and performance of the power grid [24, 25].

Discrete-time SMC is a popular control technique that is widely used in various applications due to its robustness and ability to handle system uncertainties and disturbances. One variant of SMC is the use of a desired switching variable (DSV) generator, which can improve the control performance by generating a smoother and more suitable reference signal for the sliding surface. The main objective of using a DSV generator in SMC is to achieve better tracking performance and reduce chattering, which is a common issue in traditional SMC. The DSV generator uses a dynamic model of the system and generates a continuous reference signal that is then discretized and used as the input to the SMC controller. This reference signal is then used to construct the sliding surface, which determines the control action based on the system state. The DSV generator can generate a reference signal that is more suitable for the system and can handle changes in the system dynamics more effectively. Additionally, it can reduce the chattering that is often observed in traditional SMC, which can improve the stability of the system. However, there are also some drawbacks in using a DSV generator in SMC [26, 27]. One of the main issues is the complexity of designing the DSV generator, which requires a good understanding of the system dynamics and control theory. Additionally, the DSV generator may introduce additional computational overhead and delay, which can affect the real-time performance of the system [27, 28].

The significant noise that some sliding mode controllers identify has long been a source of dissatisfaction and, in some cases, outright rejection among control designers, as sliding mode concepts recommended. Chattering is the term most commonly used to describe the occurrence. High-frequency fluctuations, referred to as chattering, emerge around the equilibrium point due to the inconsistent regulatory actions in response to the changing environment. As a consequence, many real-life applications are unable to effectively utilize the designed regulatory mechanisms to control behavior. This type of behavior gives rise to problems such as the deterioration of mechanical motion components, machine movements, fluttering use of shafts in aerospace applications, and impact during operation [27, 29, 30]. Numerous chattering preventive measures have been proposed [31–33] as a means of chattering repression. As an example, a number of researchers have been developing IM regulators based on the integration of SMC theory with other cutting-edge control techniques such as the backstepping algorithm, adaptive method, and fuzzy technique [34–36]. Subsequently, it should be noticed that using SMC in conjunction with other types of nonlinear control techniques increases controller complexities and mathematical efforts, which is not compatible with SMC's simplicity [37].

The majority of induction motor recognition algorithms depend on inaccurate induction motor appropriate variables and shortened mathematical representations [38–40]. Due to their superior learning capabilities, artificial neural

networks (ANN) are capable of overcoming this drawback. By being used to identify and manage various nonlinear and complex systems, ANN has solidified its position as a methodology. Numerous research findings, in particular, show that feed-forward ANN is successful in identifying the induction motor. It is well known that the main disadvantages of feed-forward ANNs are their lack of memory and high sensitivity to the training data because their input and outputs are solely based on the inputs and the weights used at the time [41–43]. As the architecture of the dynamic neural network (DNN) encompasses feedback from the output and has excellent interaction illustration capabilities, it can get around this drawback [44]. However, conventional static sliding mode control methods can only be applied to systems with a relative degree of one or two [45, 46]. In order to apply static sliding mode control to systems with arbitrary relative degree, an artificial delay can be introduced into the control input. This approach has been shown to be effective in controlling a variety of nonlinear systems with arbitrary relative degrees, including robotic manipulators and mechanical systems [47–49].

This study investigates the link of IM control employing SM with power steering applications. The sliding mode control mechanism and the operation of the power steering have been replicated in the simulation using virtual modules with various controllers in the interest of preserving the state's speed and torque. To further elucidate the cohabitation of these control mechanisms and the driver implementations, other simulations are also being provided. Additionally, hardware implementations are used to verify the results of simulations. The major objectives of the proposed technique are listed as follows:

(i) To develop a mathematical model for the induction motor in power steering applications, including the effects of the load and the control system

(ii) To design and train an artificial neural network for sliding mode control of the induction motor, considering the nonlinear and time-varying nature of the system

(iii) To compare the performance of the sliding mode control strategy with other control strategies, such as proportional-integral (PI) control, fuzzy logic control, and ANN control

(iv) To investigate the effect of various parameters, such as the sliding surface and the neural network architecture, on the performance of the sliding mode control strategy

(v) To evaluate the robustness of the sliding mode control strategy against disturbances, such as sudden changes in the load with the parameters of delay time, rise time, settling time, and steady-state error

(vi) To analyze the stability of the sliding mode control strategy and ensure that the closed-loop system is stable under all operating conditions

(vii) To validate the simulation results with experimental data obtained from a physical prototype of the induction motor and the power steering system

(viii) To investigate the effect of varying operating conditions, such as different steering angles and speeds, on the performance of the sliding mode control strategy

(ix) To provide insights into the practical implementation of the sliding mode control strategy, including the hardware and software requirements, and any limitations or challenges that need to be addressed

(x) To demonstrate the feasibility and effectiveness of the sliding mode control strategy for induction motors in power steering applications and to identify potential areas for future research and development

2. Indirect Vector Control of Induction Motor

Indirect vector control (IVC) is a type of control strategy which is used to control the speed regulation of induction motor (IM). By adjusting the stator current and voltage, IVC manages the motor's speed and torque. Figure 1 shows the indirect field-oriented IM schematic diagram. The three-phase currents are converted into the binary synchronous reference frame system and the synchronous frame using the Clarke and Park transforms. The feedback for the inner loops is provided by the resulting d-q axis currents. The amplitudes of the comparison dc voltages for the PWM unit with the reverse park and Clarke transform are formed by the reference amplitudes derived from the present controllers. The impulses from the PWM entity that is obtained create the trigger signals for the inverter's IGBT switching devices. In this case, the IM is fed by a PWM inverter with a hysteresis current controller. The iqs* is obtained from the speed error with the help of the PI controller, FLC, SMC, and ANN-based SMC. The ids* is obtained using essential rotating flux $\widehat{\Psi}_r$ as computed in the following equation [5]:

$$\widehat{\Psi}_r = L_m i_{ds}. \tag{1}$$

The ω_{sl}^* that is created using the current i_{qs}^* is expressed as follows [5]:

$$\omega_{sl} = \left(\frac{L_m R_r}{\widehat{\Psi} L_r}\right) \times i_{\mathrm{qs}}. \tag{2}$$

The ω_{sl}^* is summed with ω_r to ω_e. The θ_e is determined in the following equation [5]:

$$\theta_e = \int \omega_e \mathrm{dt} = \int (\omega_r + \omega_{\mathrm{sl}}). \tag{3}$$

The vector rotator converts the i_{qs}^* and i_{ds}^* to i_a^*, i_b^*, i_c^*. The measured currents are compared with the set values of the current of IM. In order to obtain the desired machine performance, the current error signal is fed to the hysteresis band. The rotational equation of a system will be transformed as follows [5]:

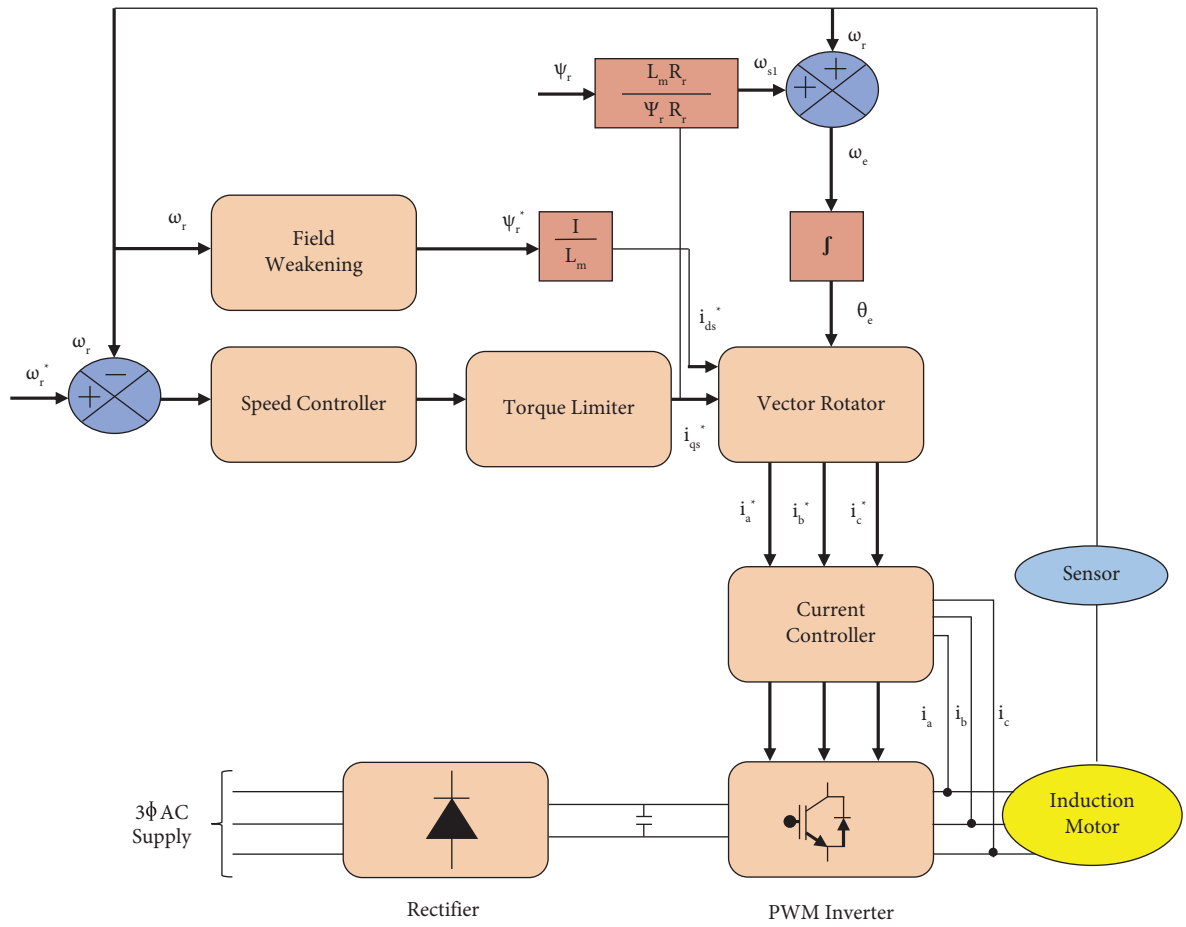

Figure 1: Indirect vector-controlled IM.

$$J\dot{\omega}(t) + B\omega_r(t) + T_L = T_e, \tag{4}$$

$$Te = \mathrm{K_t} i^*_{\mathrm{qs}}, \tag{5}$$

where K_t is the torque constant, and it is written as follows:

$$K_t = \left(\frac{3n_p}{2}\right)\left(\frac{L_m^2}{L_r}\right) i^*_{\mathrm{ds}}. \tag{6}$$

From equations (4) and (5), the mechanical equation of IM is

$$\dot{\omega}(t) = -\left(\frac{B}{J}\right)\omega \mathrm{r}(t) + \left(\frac{K_t}{J}\right)\mathrm{iqs}^*(t) - \left(\frac{1}{J}\right)\mathrm{TL}, \tag{7}$$

$$\dot{X}(t) = A_p\omega_r(t) + B_pU(t) + C_pT_L, \tag{8}$$

where $X(t) = \omega_r(t), A_p = -(B/J), B_p = K_t/J, C_p = -(I/J), U(t) = i*_{\mathrm{qs}}(t)$.

The system model uncertainties, which encompass parameter variations and external load changes, are managed by means of the induction motor (IM). Hence, a variable SMC structure is designed to enhance the performance of the IM in industries.

Rewriting equation (1) and representing the IM system without external load disturbance [12],

$$\dot{X}(t) = \mathrm{A_{pn}}\omega_{\mathrm{r}}(t) + B_{\mathrm{pn}}U(t). \tag{9}$$

By choosing the constraint changes and load torque variation, equation (9) can be rewritten as follows [12]:

$$\begin{aligned}\dot{X}(t) &= \left(A_{\mathrm{pn}} + \Delta A\right)\omega \mathrm{r}(t) + \left(B_{\mathrm{pn}} + \Delta B\right)U(t) + C_pT_L \\ &= A_{\mathrm{pn}}\omega_r(t) + B_{\mathrm{pn}}U(t) + L(t).\end{aligned} \tag{10}$$

Here, ΔA and ΔB are the uncertainties owing to model the machine variable J and B where $U(t)$ is the set speed, ω_r is measured speed of IM, and $L(t)$ is the lumped indecision as expressed in the following equation [12]:

$$L(t) = \Delta \mathrm{A}\omega_{\mathrm{r}}(t) + \Delta \mathrm{BU}(t) + C_pT_L. \tag{11}$$

3. Designing of Sliding Mode Controller with Induction Motor

3.1. Indirect Vector-Controlled IM SMC Design Circuit. Indirect vector control is achieved by generating the reference stator current vector based on the desired torque and speed of the IM. The flux vector is subsequently utilized to create the PWM signals needed to control the IM. The most widely used technique for enhancing or achieving high effectiveness in an induction motor drive is field-oriented

regulation. The methodology and the indirect method are the two fundamental types of field-oriented control. The primary difference between the two is how actuation is accomplished: the direct method uses electromagnetic or electrical feedback from the motor, whereas the implicit method uses velocity feedback from the motor and a feed-forward slip authority. Both strategies generally make use of stator existing regulations in a certain capacity. The instantaneous actuation is provided by the implicit field-oriented method using a feed-forward slip command and motor acceleration responses. Since the velocity output typically produces relatively clean input signals than the voltage from a power converter, the indirect method's control is inherently more reliable. This method differs significantly from everyone else because its outputs and evolved motor model are predicated on the motor's basic system parameters instead of a number of associated indicators. The circuit diagram of the SMC is depicted in Figure 2, where a modified vector IM is applied to signify the plant (controllable). The primary parameters of the controller have to be developed with an appropriate control law in order that the ω_r can be able to optimize ω_{r*}. In sliding mode control (SMC), the model is adjusted based on the error value (E) and the changing error (CE) variations, which are regulated using a sliding or switching surface.

Choose the sliding surface in terms of the state space equation of the model, and it is expressed in the following equation [12]:

$$s(e, \dot{e}, t) = 0. \tag{12}$$

Then, the sliding surface variables are

$$\begin{aligned} s(t) &= \ddot{e}'(t) + \lambda \bar{e}(t), \\ e(t) &= (j) r^* - \omega_r. \end{aligned} \tag{13}$$

From equation (13), the sliding surface becomes

$$\begin{aligned} \dot{\mathrm{S}}(t) &= \ddot{\mathrm{e}}\,(\acute{t}) + \lambda \dot{\mathrm{e}}(t), \\ \dot{S}(t) &= \omega_r^*(t) - A_{\mathrm{pn}} \omega_r(t) - B_{\mathrm{pn}} U(t) - L(t) + \lambda \dot{e}(t). \end{aligned} \tag{14}$$

Using the above equation, the control effort is derived as $S(t) = 0$ and $(L(t) = 0)$ is to attain the supposed characteristics of the model, and its equivalent control law is expressed in the following equation [12]:

$$U_{\mathrm{eq}}(t) = B_{\mathrm{pn}}^{-1}\left[\omega_r^* - \mathrm{A}_{\mathrm{pn}} \omega_r(t) + \lambda \dot{e}(t)\right]. \tag{15}$$

The vector control, however, responds to variables very quickly. The complex dynamics, unmodeled behaviour patterns, and impulsive variable modification adversely affect the IM's ability to control. As a result, the controller cannot guarantee any improvement in control characteristics. Thus, the support control could be developed to eradicate the unappreciable modifications. The support control effort is expressed as follows:

$$U_h(t) = g_h * \mathrm{Sgn}(S(t)), \tag{16}$$

where g_h is gain, and SMC control law is written as follows:

$$U_{\mathrm{SMC}}(t) = U_{eq}(t) + U_h(t), \tag{17}$$

$$U_h(t) = g_h \frac{(\mathrm{S}(t))}{\mathrm{S}(t)} + \gamma. \tag{18}$$

3.2. Design of ANN Controller. The input/output values are critical for training ANN in off-line IM for incoming i_{qs}^* with speed error. The variable parameters are appropriately encumbered to confirm a steady process because no supplementary learning can occur once the ANN has been trained. A feed-forward back propagation algorithm (FFBPA) is employed to train the ANN. The created model is put via the PURELIN mathematical derivation, which has a grade reduction with bias and weight updating. The learning develops in accordance with the learning requirements. The fundamental performance criterion for an ANN network is the mean square error (MSE), which should be implemented in accordance with the MSE between the target and estimated output, which has a significant impact on machine performance in ANN. In this ANN network, the least MSE that can be reached is $1e^{-5}$. In FFBPA, the differential function is used to determine the activation function (AF). The tan sigmoid function (SF), which is frequently used in squashy-restricting AF, thereby meets this requirement. The linear activation function (LAF) is utilized in output layers that never compare the output value, whereas SF is used in linear output nodes to streamline the learning process.

The fundamental concept next to SMC is to create a controller that moves the system's states towards a sliding manifold, where the complexities are more straightforward and manageable. ANNs have proven to be effective in controlling nonlinear systems, including induction motors. ANNs can approximate any nonlinear function to a desired level of accuracy, making them well-suited for control applications.

The steps to design an ANN controller for SMC of an induction motor are as follows:

Step 1: Determine the system model: The first step is to determine the mathematical model of the induction motor. This will help in understanding the dynamics of the system and developing the SMC algorithm.

Step 2: Design the sliding mode controller: The next step is to design the SMC algorithm. This involves selecting the sliding surface and designing the control law that will drive the system states towards the sliding surface.

Step 3: Train the ANN: Once the SMC algorithm is designed, an ANN can be trained to approximate the control law. The ANN should be trained using a dataset that contains the input-output pairs for the control law.

Step 4: Implement the ANN controller: The ANN can be used as an induction motor controller once it has been trained. The ANN receives the system's controller parameters as inputs and outputs the command signal that directs the system in the direction of the sliding manifold.

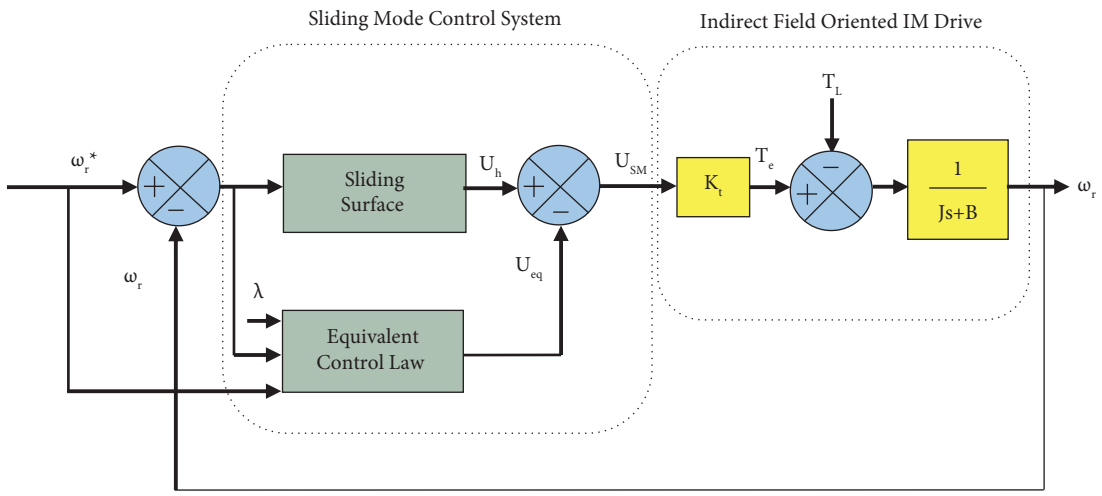

Figure 2: Design circuit of SMC for indirect vector-controlled IM.

Step 5: Test and tune the ANN controller: Finally, the ANN controller should be tested and tuned to ensure that it is performing as expected. The controller's performance can be evaluated by measuring the speed of the motor and comparing it with the desired speed.

For the hidden layer, a bipolar SF is employed, and a LAF is used for the output layer. The trials are distributed to find the lowest number of neurons required to achieve the best accuracy for each layer. The created neural network has three neurons in the hidden layer and one neuron in each of the input and output layers. Three neurons are chosen from the hidden layer to train the ANN, greatly reducing the number of epochs. In this instance, the hidden layer's simulated training data and 569 epochs of the tan sig function are shown in Figures 3 and 4.

4. Simulation Results and Discussion

The findings of designed controllers for vector-controlled IM under various operating conditions are addressed in this section. The appropriate control is designed using nonlinear mathematical analysis of an IM and the MATLAB/Simulink platform, and it implements sliding mode control for a resilient design which is resistant to variable fluctuation. When the insolation varies, the load also varies immediately. The simulated IM parameters are listed in Table 1.

In the transient region, where the output voltage is changing rapidly, a well-designed proportional-integral (PI) controller can help maintain stability and ensure that the output voltage remains within acceptable limits. Figure 5 illustrates the designed system with PI controller in transient region inverter output voltage 460 V peak value. The rotor speed is seamlessly changed, the stator current has a frequency response form, and the amplitude of the stator flux linkage is continuous from the dynamic response procedure of the speed regression. It demonstrates that the suggested method exhibits an acceptable dynamic characteristic. Figure 6 illustrates the PI controller in a transient region speed of 118 (rad/sec) with a settling time of 6 sec. The torque needed to initiate a motor's rotation is known as the

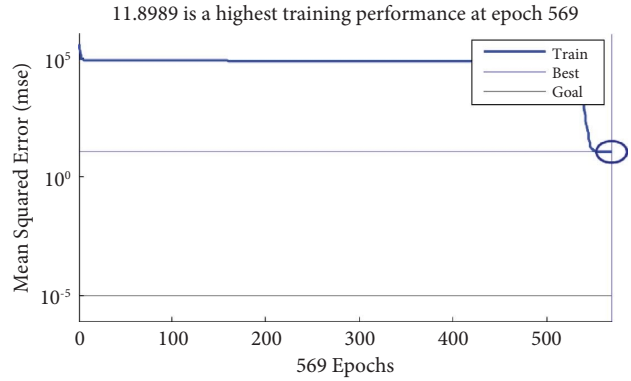

Figure 3: Optimal point in ANN for IM.

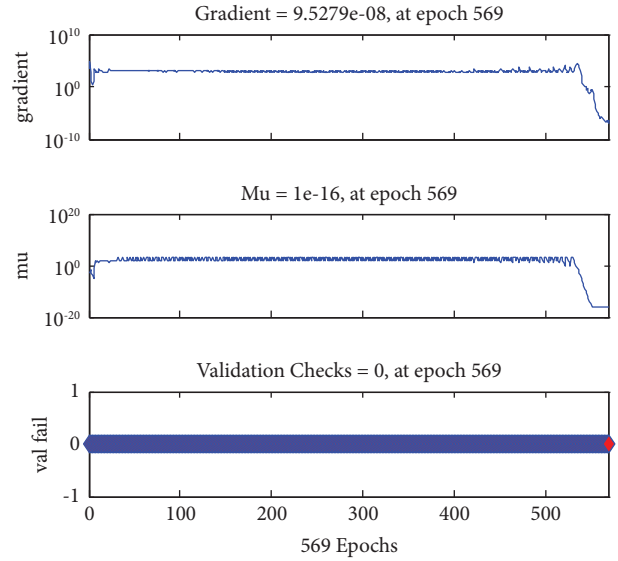

Figure 4: Training algorithm of IM.

electromagnetic torque, and it is typically equal to the load torque. For a system with a PI controller in the transient region, such as a speed control system, the controller's

Table 1: Simulated parameters of IM.

Parameters	Values
Power	30 HP
Voltage	460 V
Stator resistance	0.087 ohms
Stator inductance	0.8×10^{-3} H
Rotor resistance	0.228 ohms
Rotor inductance	0.8×10^{-3} H
Mutual inductance	34.7×10^{-3} H
Moment of inertia	1.662 kg-m^2
Pole pairs	2

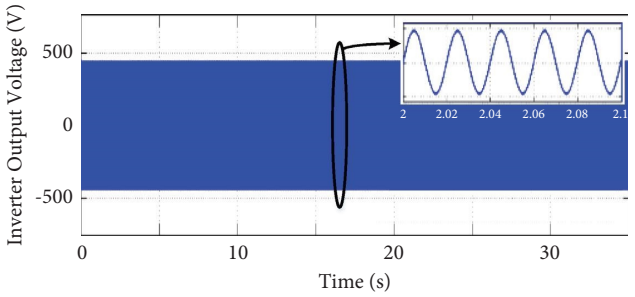

Figure 5: Designed system with PI controller in transient region inverter output voltage.

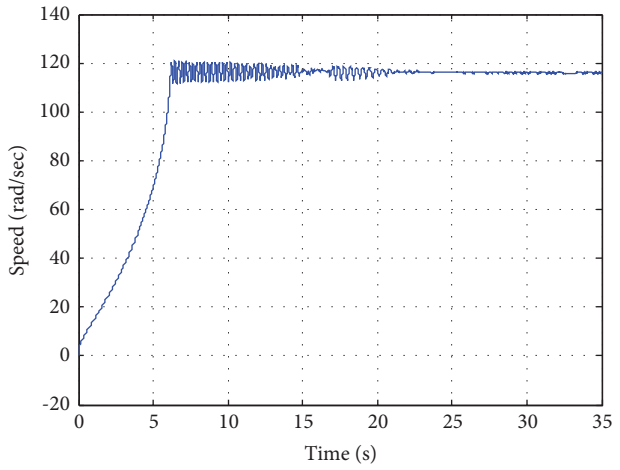

Figure 6: Designed system with PI controller in transient region speed (rad/sec).

output is determined by the error between the desired speed and the actual speed of the system. The proportional term of the controller responds to the current error, while the integral term responds to the historical error. In order to design a PI controller for a speed control system in the transient region, the first step is to determine the transfer function of the system. This can be performed by analysing the dynamics of the system and deriving an equation that relates the output of the system (the speed) to the input (the control signal). In a load variation from electromagnetic torque of 10 N-m to 5 N-m, Figure 7 shows the simulated results of a designed system with a PI controller. After 20 seconds of operation, the torque is settled according to the observation.

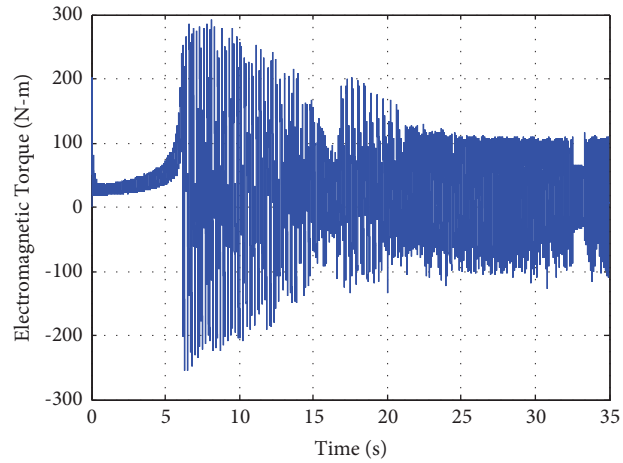

Figure 7: Simulated results of designed system with PI controller in load variation from electro-magnetic torque varied from 10 N-m to 5 N-m.

Figure 8 shows the results of a designed system with a PI controller in terms of load variation speed (rad/sec). The range of the load torque has to be located from 5 to 10 N-m. The load's oscillations have already subsided, and the load torque disturbance has decreased from a maximum variation of 10 to 5 N-m after 20 seconds. The simulated outcomes of the designed system with the PI controller are shown in Figure 9 in terms of load variation speed (rad/sec). The range of the load torque has to be located from 5 to 10 N-m. After 20 seconds, the IM's speed has controlled after experiencing oscillations with a value of 120 rad/sec. Due to the voltage drop caused by the excitation of the stator and rotor windings, the DC voltage has been reduced from 460 V to 420 V while the PI controller had been able to operate.

SMC, a nonlinear control technique, forces a nonlinear system to slide along a cross section of its appropriate behaviour by implementing a discrete control signal (or, more precisely, a collection control signal). Figure 10 illustrates the simulated results of the designed system with PI controller inverter output voltage with the variation of 460 V to 420 V after 28 seconds. Figure 11 illustrates the speed results of the designed system with fuzzy sliding-mode controller (FSMC) in load variation with sliding surface according to control law. According to the measured and reference speed values, Figure 12 shows the simulated speed results of the designed system with ANN-based SMC in the speed reversal from 116 rad/sec to −116 rad/sec. The speed variation of various controllers for PI, SMC, FLC with SMC, and ANN with SMC is shown in Figure 13. When compared to other algorithms, ANN with SMC performs faster and with less load disturbance. Table 2 compares the various speed parameters in terms of error value for delay time, rise time, peak time, and settling time. In terms of performance, ANN with SMC has performed better due to its lower error value in terms of the controller.

The voltage, current, speed, and torque results of a power steering control system designed based on SMC will depend on the specific design parameters and system characteristics. SMC is a reliable control method which, in the absence of

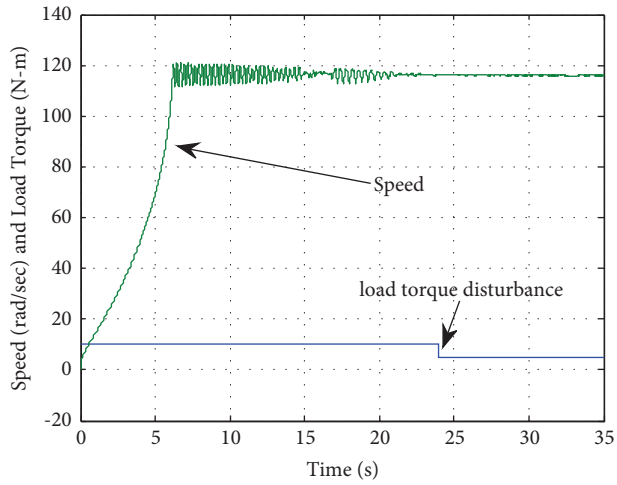

Figure 8: Simulated results of designed system with PI controller in load variation speed (rad/sec) from load torque varied from 5 N-m to 10 N-m.

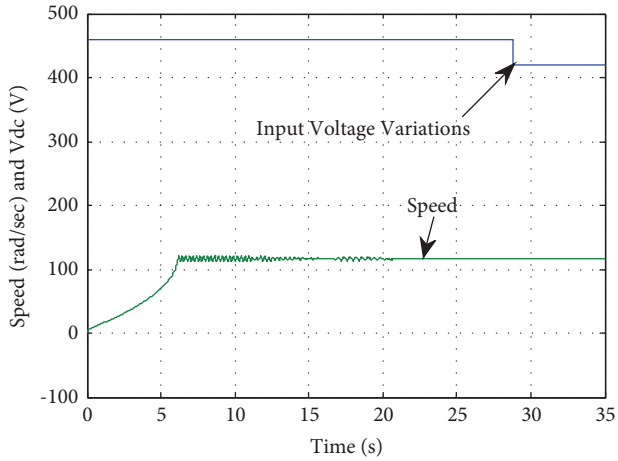

Figure 9: Simulated results of designed system with PI controller in line voltage variation from 460 V to 420 V.

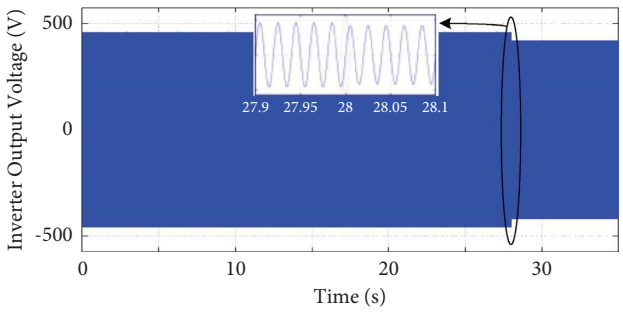

Figure 10: Simulated results of designed system with PI controller inverter output voltage.

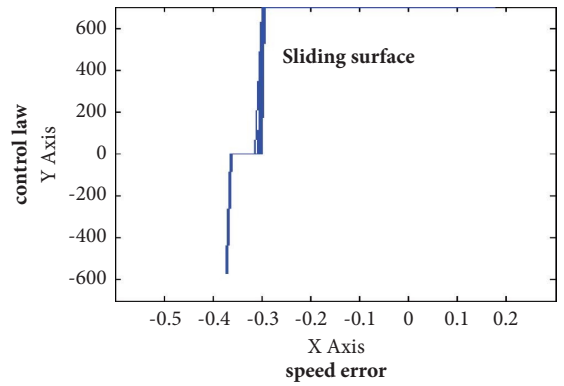

Figure 11: Simulated speed results of designed system with FSMC in load variation with sliding surface.

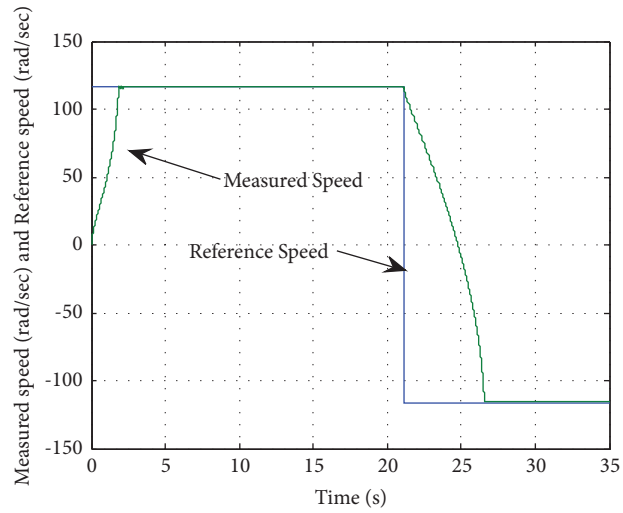

Figure 12: Simulated speed results of designed system with ANN-based SMC in speed reversal from 116 rad/sec to −116 rad/sec.

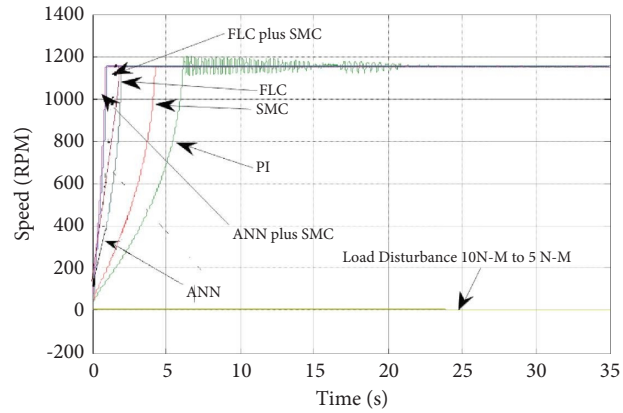

Figure 13: Comparison of speed in various controllers.

system disturbances and unpredictability, can deliver good detection accuracy. In a power steering control system, the voltage and current will depend on the power source and motor specifications, as well as the load on the system. The speed and torque of the motor will be influenced by the control inputs and the mechanical properties of the system, such as the gear ratio and steering mechanism. If the SMC design is successful, it should be able to regulate the voltage and current to provide stable power to the motor, while also controlling the speed and torque to achieve the desired

Table 2: Comparison table of speeds in various controllers.

Controllers	T_d (sec)	T_r (sec)	T_p (sec)	T_s (sec)	Errors
PI control	4.4	6.0	7.0	22	0.68
SMC	3.0	4.4	4.6	5.1	0.098
Fuzzy	2.0	2.4	2.6	3.0	0.13
Fuzzy plus SMC	1.2	1.4	1.8	2.0	0.1
ANN	1.0	2.0	2.3	2.5	0.08
ANN plus SMC	0.8	1.2	1.6	1.7	0.05

Table 3: Comparisons for SMC and ANN-based SMC power steering.

Controllers	T_d (sec)	T_r (sec)	T_p (sec)	T_s (sec)	Error
SMC	0.5	0.8	0.9	1.4	0.357
ANN plus SMC	0.4	0.7	0.8	0.9	0.111

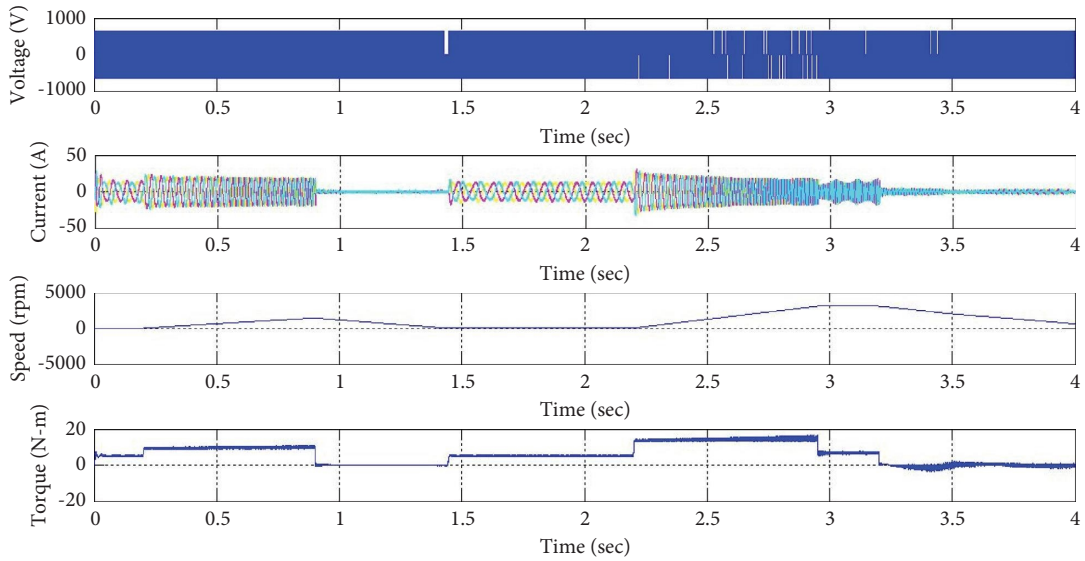

Figure 14: Simulated voltage, current, speed, and torque results of designed system-based SMC in power steering control.

steering performance. The exact values of these variables will depend on the specific system design and operating conditions.

Table 2 illustrates the comparative analysis of various controllers under different torque conditions. The SMC and ANN-based SMC are applied to the power steering application of IM. In comparison of the abovementioned two controllers, the ANN-based SMC gives improved performance. Table 3 illustrates the proposed sliding mode controller with the ANN approach, which gives a lesser error value than without SMC. For the designed system-based SMC in power steering control, where the voltage value has been varied from 460 to −460 V, Figure 14 shows the voltage, current, speed, and torque. Specifically, the delay time, rise time, peak time, and settling time have all been varied for the current parameter. After varying over time, the induction motor's speed and torque have finally been controlled. Figure 15 shows the voltage, current, speed, and torque results of the designed system with ANN-based SMC, which have smoother results as a result of the system's inclusion of ANN. A power steering control system can be designed using SMC to regulate the current and flux parameters. The SMC algorithm is robust to disturbances and can guarantee system stability and tracking performance. The simulation results of the designed system with SMC in power steering control are shown in Figure 16 for the parameters current and flux.

5. Experimental Setup and Validation

The hardware test was conducted to confirm the viability of the suggested control strategy. The exact same motor parameters that were used here were additionally employed in the simulation as shown in Table 1. The PM75RL1A060 (Mitsubishi) IPM modules and the TMS320F28335 control board have been combined to form an inverter (Texas Instrument). Four current sensors (two for each motor) and one voltage sensor were also used to keep track of the DC-link voltage and motor currents. The machine, which is robotically combined with the drive shaft, has a resistor connected through the diode rectifier to interact with the load application. The experimental model of the designed system is shown in Figure 17.

The time response of PWM pulses for an inverter can be characterized by two important parameters, T_{ON} and T_{OFF}. T_{ON} refers to the time duration for which the pulse remains

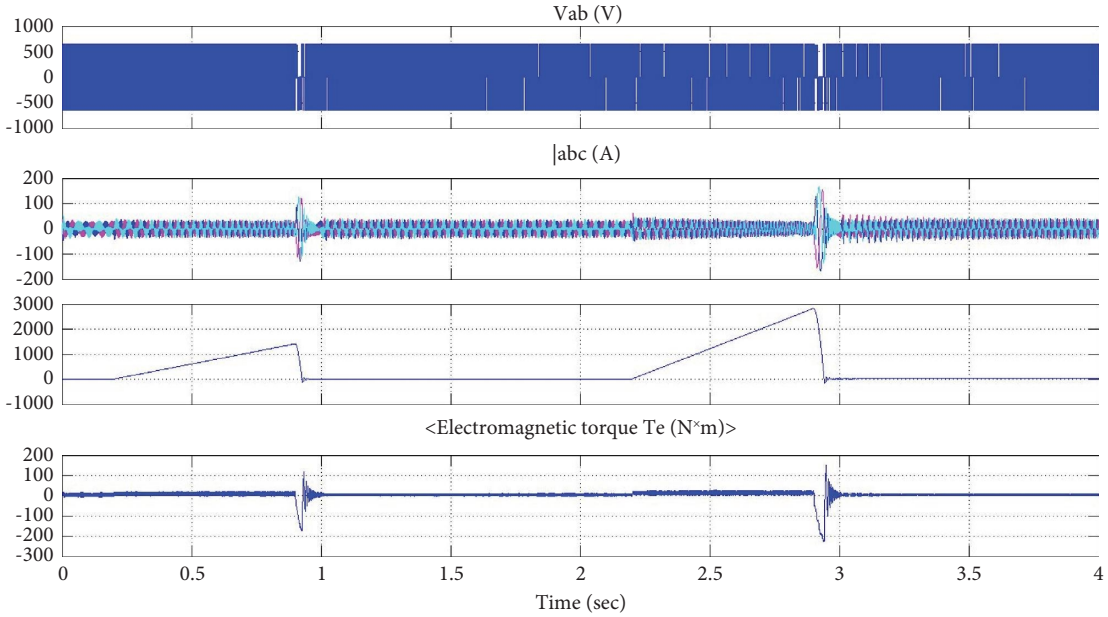

Figure 15: Simulated voltage, current, speed, and torque results of designed system with ANN-based SMC in power steering control.

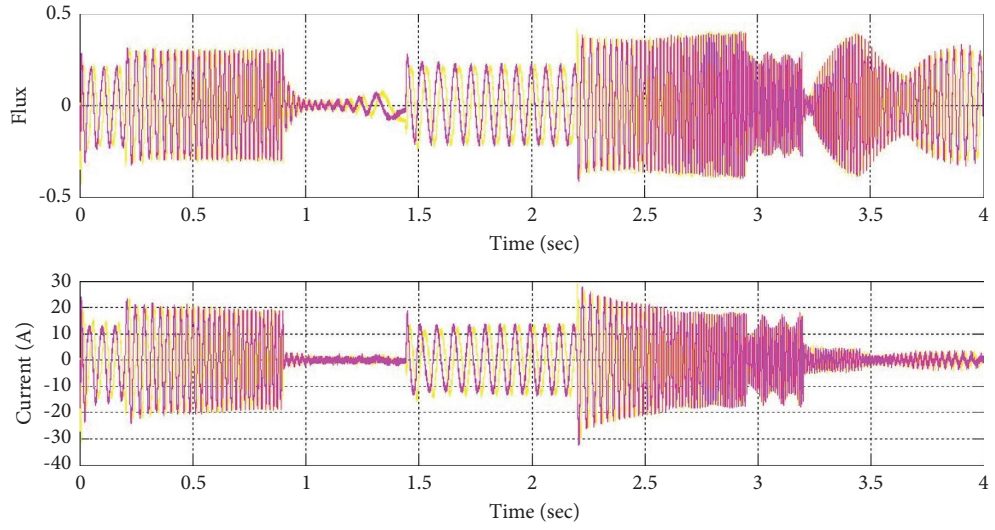

Figure 16: Simulated results of the designed system with SMC in power steering control for the parameters current and flux.

ON, while T_{OFF} refers to the time duration for which the pulse remains OFF. The ratio of T_{ON} to the total time period of the pulse is called the duty cycle, and it determines the average power delivered to the load. For example, if the pulse has a total time period of T, and T_{ON} is equal to 0.4 T, then the duty cycle would be 0.4. This means that the pulse is ON for 40% of the time and OFF for 60% of the time. The T_{ON} and T_{OFF} times are determined by the input signal to the inverter's PWM controller. The controller compares the input signal with a triangular waveform of fixed frequency and generates a PWM output signal whose duty cycle is proportional to the amplitude of the input signal. The T_{ON} and T_{OFF} times can also affect the harmonic value of the voltage output patterns, which is important in applications such as motor control. In general, the T_{ON} and T_{OFF} times are chosen such that the voltage output waveform has a low harmonic distorted value and the average power delivered to the load is as desired. The exact values of T_{ON} and T_{OFF} may vary depending on the specific application and the characteristics of the load. Table 4 displays the induction motor's acceleration time T_1, turning time T_2, and deceleration time T_3 throughout the operation. The PWM technique has been used to drive an induction motor by controlling an inverter. The on-and-off periods of this PWM pulse can be provided by the sliding mode estimation and the input (angle from steering). The acceleration time is determined by the time at which the angle is reached. The angle needs to be reached because the input determines when to turn on.

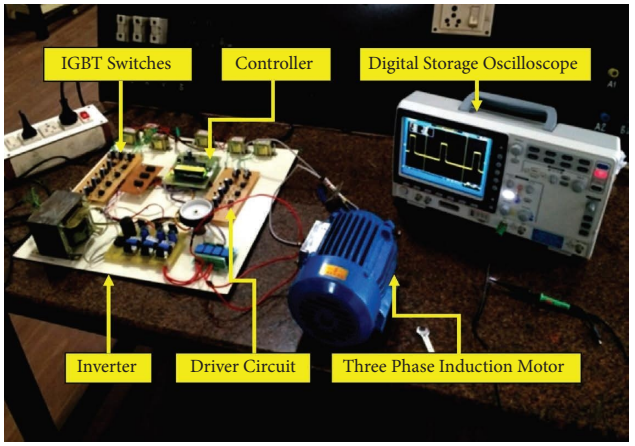

Figure 17: Experimental model.

Table 4: T_{ON}/T_{OFF} time response of PWM pulse for the inverter.

Angle (degree)	Time (sec)	T_1 (sec)	T_2 (sec)	T_3 (sec)
35	9	5.5	10	4.5
50	11	7	9	5
100	9	8	16	6.5
175	22	9.5	20	4

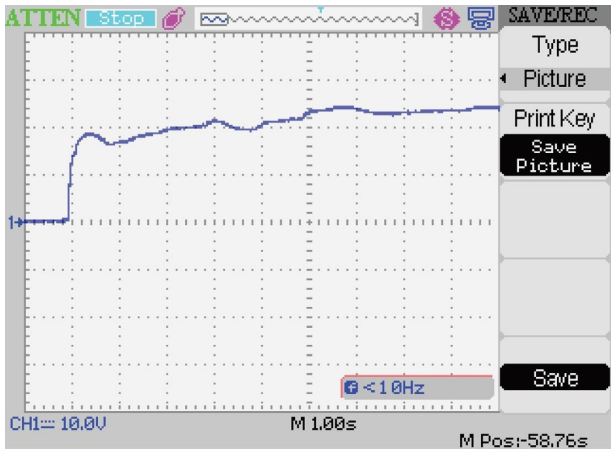

Figure 18: Fuzzy logic controller-based IM—speed.

Table 5: Induction motor parameters.

Parameters	Values
Power	5.4 HP
Voltage	400 V
Frequency	50 Hz
Stator resistance	1.405 Ω
Stator inductance	0.0058 H
Rotor resistance	1.395 Ω
Rotor inductance	0.0058 H
Mutual inductance	0.172 H
Inertia	0.0131 kg-m^2

The fuzzy logic controller-based 1800 rpm induction motor speed is shown in Figure 18. This is possible because the fuzzy logic controller only has one pole,

Table 6: Three-phase inverter configuration.

Parameters	Values
Number of phases	3
Number and type of switch	6 & IGBT
Inverter inductance	5.0 mH
Grid side inductance	3.0 mH
Switching frequency	10 kHz
Dead time	2 μs
Maximum DC bus voltage	500 V
Rated AC current (peak)	25 A
Rated AC voltage (peak)	220 V
Rated power	100 kW
Filter capacitor	92 μF

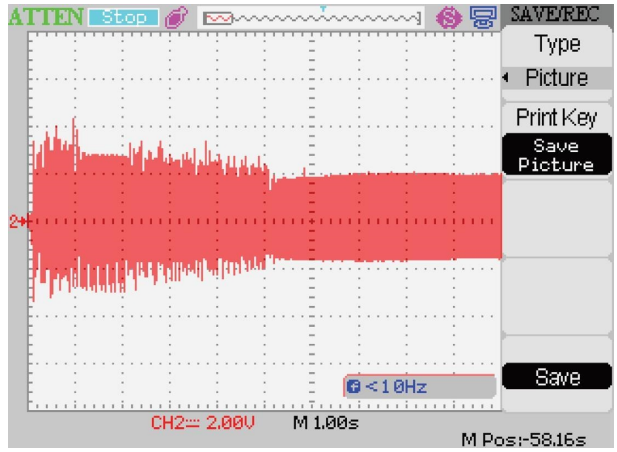

Figure 19: Fuzzy logic controller-based IM—current.

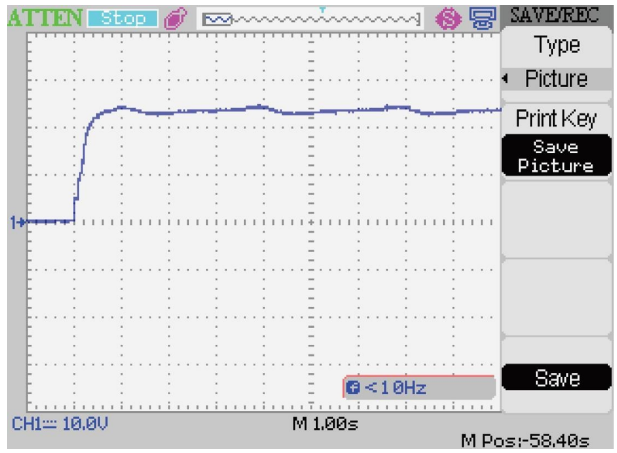

Figure 20: Sliding mode controller-based IM—speed.

allowing it to control the system independently of the other poles. According to the inspection in the figure, the system's speed varies every second. With PI and PID, however, stability could not be maintained when a setting point lower than the appropriate setting point (1800 rpm) has been applied. This is due to the regulation having multiple poles, so when the setting point is intended from the start, the control system can only preserve the way to

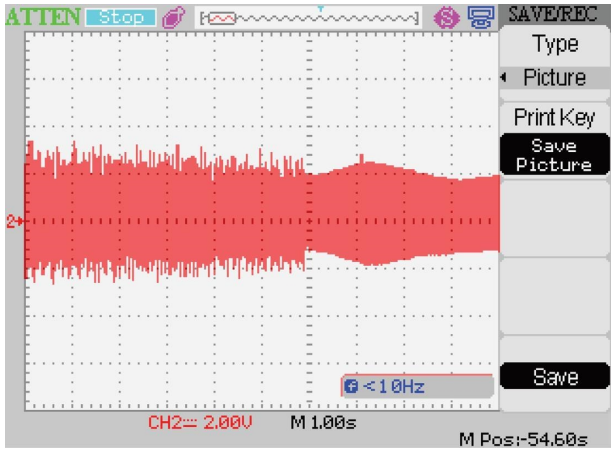

Figure 21: Sliding mode controller-based IM—current.

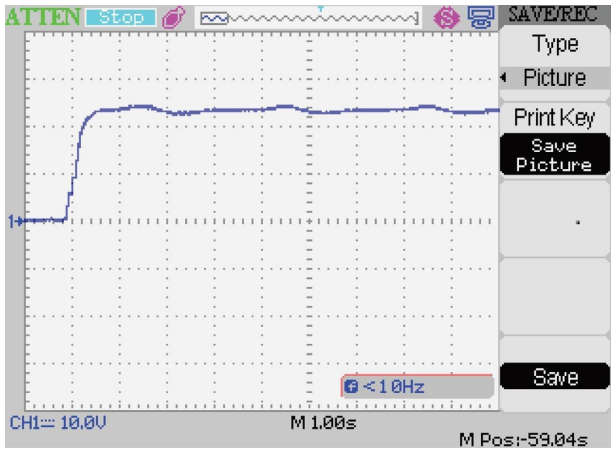

Figure 22: ANN-based sliding mode controller-based IM—speed.

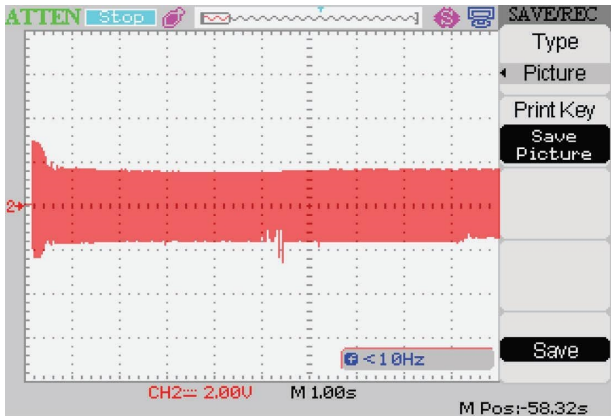

Figure 23: ANN-based sliding mode controller-based IM—current.

set the position in that region. Tables 5 and 6 illustrate induction motor parameters and three-phase induction motors of the experimental setup.

Figure 19 depicts the output of a fuzzy logic controller-based induction motor current, which indicates the stator current at 75% of the load condition.

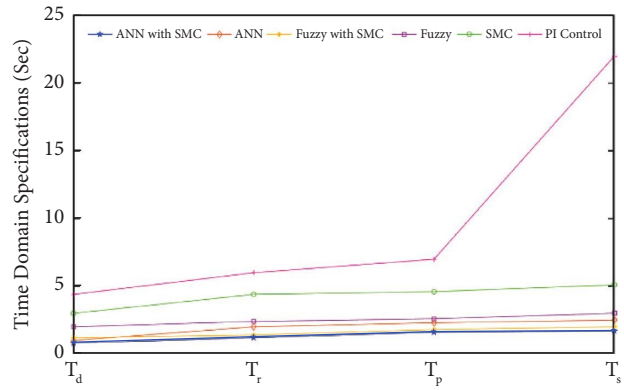

Figure 24: Comparative analysis of various controllers with time domain specifications.

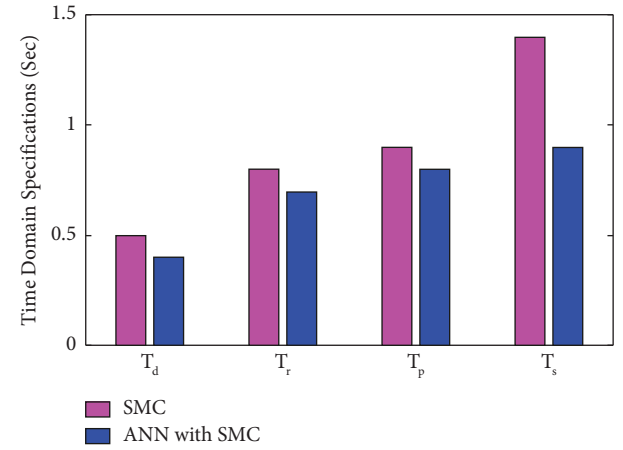

Figure 25: Comparative analysis of SMC and interference of ANN.

The respondents of an induction motor based on a sliding mode controller under steady state speed conditions are shown in Figure 20. The P-I controller's speed response is directly impacted by the load disturbance; meanwhile, the sliding mode controller has demonstrated its reliability against load fluctuations. Figure 21 depicts the output of a sliding mode controller induction motor current, which indicates the stator current at 75% of the load condition. The induction motor with speed controller is designed based on a sliding mode controller as shown in Figure 22. When a load is applied, the ANN-based sliding controller exhibits a considerable portion of motor speed gradation. The ANN controller responds more quickly than the fuzzy controller. Figure 23 shows an induction motor with a sliding mode controller based on an ANN with a smaller ripple than a sliding mode or fuzzy logic controller for the current value.

Figure 24 depicts, from the inspection of various time periods, the time domain specifications of the delay time, rise time, peak time, and settling time characteristics of PI control, sliding mode control, fuzzy, fuzzy with SMC, ANN control, and ANN with SMC. From the characteristics, it can be contended that ANN with sliding mode control performs better than other controllers. The interference of the ANN

technique in power steering sliding mode control applications is shown in Figure 25.

6. Conclusion

In this study, a novel sliding mode speed controller using ANN for induction motor drives fed by a voltage source inverter is investigated. The disruption observation estimates a continuous input disturbance signal with the purpose of mitigating it in the SMC algorithm. As a consequence, sliding mode controllers integrate processors into their designs implicitly. Using sliding mode control for flux estimation, this work has devised a plan for enhancing the response qualities of a power steering induction motor. For the system, the suggested technique calculates and estimates the speed, torque, and electrical angle. Furthermore, simulation data are provided to validate and demonstrate the feasibility of the proposed approach. Moreover, the concept of power steering combined with sliding mode control for a three-phase induction motor is examined, and its efficacy is examined. The proposed sliding mode control systems are compared to other controllers using experimental data, and the results show that ANN-based sliding mode control has better value in terms of delay time, rising time, peak time, and settling time.

Data Availability

The data supporting the current study are available from the corresponding author upon request.

Conflicts of Interest

The authors declare that there are no conflicts of interest.

Authors' Contributions

All authors contributed equally to this study.

References

[1] L. Djilali, A. Badillo-Olvera, Y. Yuliana Rios, H. López-Beltrán, and L. Saihi, "Neural high order sliding mode control for doubly fed induction generator based wind turbines," *IEEE Latin America Transactions*, vol. 20, no. 2, pp. 223–232, 2022.

[2] G. Fuhui and L. Pingli, "Fast self-adapting high-order sliding mode control for a class of uncertain nonlinear systems," *Journal of Systems Engineering and Electronics*, vol. 32, no. 3, pp. 690–699, 2021.

[3] Y. Han, S. Chen, C. Gong, X. Zhao, F. Zhang, and Y. Li, "Accurate SM disturbance observer-based demagnetization fault diagnosis with parameter mismatch impacts eliminated for IPM motors," *IEEE Transactions on Power Electronics*, vol. 38, no. 5, pp. 5706–5710, 2023.

[4] J. Guo, "The load frequency control by adaptive high order sliding mode control strategy," *IEEE Access*, vol. 10, pp. 25392–25399, 2022.

[5] N. Vaishnav and A. K. Jain, "Stabilizing sets of current PI controllers for IM drives with and without LC filter," *IEEE Transactions on Energy Conversion*, vol. 37, no. 2, pp. 958–969, 2022.

[6] W. A. Apaza-Perez, A. Girard, C. Combastel, and A. Zolghadri, "Symbolic observer-based controller for uncertain nonlinear systems," *IEEE Control Systems Letters*, vol. 5, no. 4, pp. 1297–1302, 2021.

[7] B. Wang, T. Wang, Y. Yu, and D. Xu, "Second-order terminal sliding-mode speed controller for induction motor drives with nonlinear control gain," *IEEE Transactions on Industrial Electronics*, vol. 70, no. 11, pp. 10923–10934, 2023.

[8] R. Tarvirdilu-Asl, S. Nalakath, Z. Xia, Y. Sun, J. Wiseman, and A. Emadi, "Improved online optimization-based optimal tracking control method for induction motor drives," *IEEE Transactions on Power Electronics*, vol. 35, no. 10, pp. 10654–10672, 2020.

[9] G. Rinaldi, P. P. Menon, C. Edwards, and A. Ferrara, "Sliding mode observer-based finite time control scheme for frequency regulation and economic dispatch in power grids," *IEEE Transactions on Control Systems Technology*, vol. 30, no. 3, pp. 1296–1303, 2022.

[10] R. Rai, S. Shukla, and B. Singh, "Sensorless field oriented SMCC based integral sliding mode for solar PV based induction motor drive for water pumping," *IEEE Transactions on Industry Applications*, vol. 56, no. 5, pp. 5056–5064, 2020.

[11] X. Lin, Y. Wen, R. Yu, J. Yu, and H. Wen, "Improved weak grids synchronization unit for passivity enhancement of grid-connected inverter," *IEEE Journal of Emerging and Selected Topics in Power Electronics*, vol. 10, no. 6, pp. 7084–7097, 2022.

[12] N.-D. Nguyen, N. N. Nam, C. Yoon, and Y. I. Lee, "Speed sensorless model predictive torque control of induction motors using a modified adaptive full-order observer," *IEEE Transactions on Industrial Electronics*, vol. 69, no. 6, pp. 6162–6172, 2022.

[13] B. Çavuş and M. Aktaş, "MPC-based flux weakening control for induction motor drive with DTC for electric vehicles," *IEEE Transactions on Power Electronics*, vol. 38, no. 4, pp. 4430–4439, 2023.

[14] X. Lin, Y. Liu, J. Yu, R. Yu, J. Zhang, and H. Wen, "Stability analysis of Three-phase Grid-Connected inverter under the weak grids with asymmetrical grid impedance by LTP theory in time domain," *International Journal of Electrical Power & Energy Systems*, vol. 142, Article ID 108244, 2022.

[15] Y. Gao, M. Doppelbauer, J. Ou, and R. Qu, "Design of a double-side flux modulation permanent magnet machine for servo application," *IEEE Journal of Emerging and Selected Topics in Power Electronics*, vol. 10, no. 2, pp. 1671–1682, 2022.

[16] X. Yang and X. Zheng, "Gradient descent algorithm-based adaptive NN control design for an induction motor," *IEEE Transactions on Systems, Man, and Cybernetics: Systems*, vol. 51, no. 2, pp. 1027–1034, 2021.

[17] C. Chen, X. Wu, X. Yuan, and X. Zheng, "A new technique for the subdomain method in predicting electromagnetic performance of surface-mounted permanent magnet motors with shaped magnets and a quasi-regular polygon rotor core," *IEEE Transactions on Energy Conversion*, vol. 38, no. 2, pp. 1396–1409, 2023.

[18] O. Gulbudak, M. Gokdag, and H. Komurcugil, "Model predictive control strategy for induction motor drive using lyapunov stability objective," *IEEE Transactions on Industrial Electronics*, vol. 69, no. 12, pp. 12119–12128, 2022.

[19] X. Zhang, Z. Wang, and Z. Lu, "Multi-objective load dispatch for microgrid with electric vehicles using modified gravitational search and particle swarm optimization algorithm," *Applied Energy*, vol. 306, Article ID 118018, 2022.

[20] T.-I. Yeam and D. C. Lee, "Design of sliding-mode speed controller with active damping control for single-inverter dual-PMSM drive systems," *IEEE Transactions on Power Electronics*, vol. 36, no. 5, pp. 5794–5801, 2021.

[21] X. Zhang, Z. Lu, X. Yuan, Y. Wang, and X. Shen, "L2-Gain adaptive robust control for hybrid energy storage system in electric vehicles," *IEEE Transactions on Power Electronics*, vol. 36, no. 6, pp. 7319–7332, 2021.

[22] G. Tu, Y. Li, and J. Xiang, "Sliding mode control of energy storage systems for reshaping the accelerating power of synchronous generators," *IEEE Transactions on Power Systems*, vol. 38, no. 2, pp. 1242–1256, 2023.

[23] B. Wang, D. Zhu, L. Han, H. Gao, Z. Gao, and Y. Zhang, "Adaptive Fault-tolerant control of a hybrid canard rotor/wing UAV under transition flight subject to actuator faults and model uncertainties," *IEEE Transactions on Aerospace and Electronic Systems*, vol. 59, no. 4, pp. 4559–4574, 2023.

[24] T. Ahmed, A. Waqar, R. M. Elavarasan, J. Imtiaz, M. Premkumar, and U. Subramaniam, "Analysis of fractional order sliding mode control in a D-STATCOM integrated power distribution system," *IEEE Access*, vol. 9, pp. 70337–70352, 2021.

[25] Y. Lu, C. Tan, W. Ge, Y. Zhao, and G. Wang, "Adaptive disturbance observer-based improved super-twisting sliding mode control for electromagnetic direct-drive pump," *Smart Materials and Structures*, vol. 32, no. 1, Article ID 017001, 2023.

[26] A. Bartoszewicz and K. Adamiak, "Discrete-time sliding-mode control with a desired switching variable generator," *IEEE Transactions on Automatic Control*, vol. 65, no. 4, pp. 1807–1814, 2020.

[27] H. Wang, X. Wu, X. Zheng, and X. Yuan, "Model predictive current control of nine-phase open-end winding PMSMs with an online virtual vector synthesis strategy," *IEEE Transactions on Industrial Electronics*, vol. 70, no. 3, pp. 2199–2208, 2023.

[28] Y. Wu, S. E. Li, J. Cortés, and K. Poolla, "Distributed sliding mode control for nonlinear heterogeneous platoon systems with positive definite topologies," *IEEE Transactions on Control Systems Technology*, vol. 28, no. 4, pp. 1272–1283, 2020.

[29] L. Hou, J. Ma, and W. Wang, "Sliding mode predictive current control of permanent magnet synchronous motor with cascaded variable rate sliding mode speed controller," *IEEE Access*, vol. 10, pp. 33992–34002, 2022.

[30] H. Lin, J. Liu, X. Shen et al., "Fuzzy sliding-mode control for three-level NPC afe rectifiers: a chattering alleviation approach," *IEEE Transactions on Power Electronics*, vol. 37, no. 10, pp. 11704–11715, 2022.

[31] S. Liu, Z. Song, Y. Liu, Y. Chen, and C. Liu, "Flux-weakening controller design of dual three-phase PMSM drive system with copper loss minimization," *IEEE Transactions on Power Electronics*, vol. 38, no. 2, pp. 2351–2363, 2023.

[32] S. V. Malge, M. G. Ghogare, S. L. Patil, A. S. Deshpande, and S. K. Pandey, "Chatter-free non-singular fast terminal sliding mode control of interleaved boost converter," *IEEE Transactions on Circuits and Systems II: Express Briefs*, vol. 70, no. 1, pp. 186–190, 2023.

[33] S. Liu and C. Liu, "Virtual-vector-based robust predictive current control for dual three-phase PMSM," *IEEE Transactions on Industrial Electronics*, vol. 68, no. 3, pp. 2048–2058, 2021.

[34] S. Liu and C. Liu, "Direct harmonic current control scheme for dual three-phase PMSM drive system," *IEEE Transactions on Power Electronics*, vol. 36, no. 10, pp. 11647–11657, 2021.

[35] S. Liu, C. Liu, H. Zhao, Y. Liu, and Z. Dong, "Improved flux weakening control strategy for five-phase PMSM considering harmonic voltage vectors," *IEEE Transactions on Power Electronics*, vol. 37, no. 9, pp. 10967–10980, 2022.

[36] W. Xu, S. Qu, and C. Zhang, "Fast terminal sliding mode current control with adaptive extended state disturbance observer for PMSM system," *IEEE Journal of Emerging and Selected Topics in Power Electronics*, vol. 11, no. 1, pp. 418–431, 2023.

[37] K. Liao, D. Lu, M. Wang, and J. Yang, "A low-pass virtual filter for output power smoothing of wind energy conversion systems," *IEEE Transactions on Industrial Electronics*, vol. 69, no. 12, pp. 12874–12885, 2022.

[38] S. Xu, H. Dai, L. Feng, H. Chen, Y. Chai, and W. X. Zheng, "Fault estimation for switched interconnected nonlinear systems with external disturbances via variable weighted iterative learning," *IEEE transactions on circuits and systems II: Express briefs*, vol. 70, no. 6, pp. 2011–2015, 2023.

[39] Y. Xu, S. Li, and J. Zou, "Integral sliding mode control based deadbeat predictive current control for PMSM drives with disturbance rejection," *IEEE Transactions on Power Electronics*, vol. 37, no. 3, pp. 2845–2856, 2022.

[40] V. K. Dunna, K. P. B. Chandra, P. K. Rout, and B. K. Sahu, "Design and real-time validation of higher order sliding mode observer-based integral sliding mode MPPT control for a DC microgrid," *IEEE Canadian Journal of Electrical and Computer Engineering*, vol. 45, no. 4, pp. 418–425, 2022.

[41] D. Li, S. S. Ge, and T. H. Lee, "Fixed-time-synchronized consensus control of multiagent systems," *IEEE transactions on control of network systems*, vol. 8, no. 1, pp. 89–98, 2021.

[42] J. Fei and H. Wang, "Experimental investigation of recurrent neural network fractional-order sliding mode control of active power filter," *IEEE Transactions on Circuits and Systems II: Express Briefs*, vol. 67, no. 11, pp. 2522–2526, 2020.

[43] W. Deng, Y. Zhang, Y. Tang, Q. Li, and Y. Yi, "A neural network-based adaptive power-sharing strategy for hybrid frame inverters in a microgrid," *Frontiers in Energy Research*, vol. 10, 2023.

[44] X. Ma, Y. Wan, Y. Wang et al., "Multi-parameter practical stability region analysis of wind power system based on limit cycle amplitude tracing," *IEEE Transactions on Energy Conversion*, vol. 2023, Article ID 3274775, 13 pages, 2023.

[45] J. Xu, E. Fridman, L. Fridman, and Y. Niu, "Static sliding mode control of systems with arbitrary relative degree by using artificial delay," *IEEE Transactions on Automatic Control*, vol. 65, no. 12, pp. 5464–5471, 2020.

[46] W. Sun, H. Wang, and R. Qu, "A novel data generation and quantitative characterization method of motor static eccentricity with adversarial network," *IEEE Transactions on Power Electronics*, vol. 38, no. 7, pp. 8027–8032, 2023.

[47] A. Taghieh, A. Mohammadzadeh, C. Zhang, N. Kausar, and O. Castillo, "A type-3 fuzzy control for current sharing and voltage balancing in microgrids," *Applied Soft Computing*, vol. 129, Article ID 109636, 2022.

[48] W. Zhang, C. Yan, X. Liu et al., "Global characterization of megakaryocytes in bone marrow, peripheral blood, and cord blood by single-cell RNA sequencing," *Cancer Gene Therapy*, vol. 29, no. 11, pp. 1636–1647, 2022.

[49] G. Bartolini and E. Punta, "Multi-input sliding mode control of nonlinear uncertain non-affine systems with monodirectional actuation," *IEEE Transactions on Automatic Control*, vol. 60, no. 2, pp. 393–403, 2015.